



A comparative study of different references for EEG default mode network: The use of the infinity reference

Yun Qin, Peng Xu, Dezhong Yao *

Key Laboratory for NeuroInformation of Ministry of Education, School of Life Science and Technology, University of Electronic Science and Technology of China, Chengdu 610054, China

See Editorial, pages 1973–1975

ARTICLE INFO

Article history:

Accepted 15 March 2010

Available online 12 June 2010

Keywords:

EEG reference

Power spectra

Coherence

Connectivity

DMN

Frequency bands

ABSTRACT

Objective: The choice of electroencephalograph (EEG) reference is a critical issue for the study of brain activity. The present study addressed the use of the infinity reference obtained by the reference electrode standardisation technique (REST) in the study of EEG default mode network (DMN).

Methods: A total of 100 randomly positioned source configurations, each consisting of two dipoles with coherent waveforms, were adopted for simulating EEG networks. Dense (129-channel), eyes-closed EEG was recorded from 15 subjects. Simulated data with infinity as reference and the real data were re-referenced to reconstructed infinity (REST), their average (AR), linked mastoids (LM) and left mastoid (L) references. For simulated data, the effects of different references on coherence and network were investigated. For real data, spectral properties of seven conventional EEG frequency bands were first analysed and then DMN was constructed based on the coherence.

Results: The simulation showed that REST can exactly recover the true EEG network configuration. For real EEG data, significant differences among references were found for the power spectra, coherence and DMN configuration. Compared with REST, the long-distance connectivity between anterior and posterior areas was strengthened by AR, and the connectivity over posterior areas was destroyed when LM and L were employed. Moreover, all comparisons demonstrated frequency-dependent reference effects.

Conclusions: Non-neutral reference influences the power spectra, coherence as well as the network analysis. REST demonstrates its validity in data referencing, and meanwhile, AR is much closer to REST than the other references in terms of spectra and coherence. However, the DMN alters a great deal with AR.

Significance: The results underscore the importance of considering EEG reference effects in the functional connectivity studies. REST is a promising reference technique for objective comparison in cross-laboratory studies and clinical practices.

© 2010 International Federation of Clinical Neurophysiology. Published by Elsevier Ireland Ltd. All rights reserved.

1. Introduction

The choice of electroencephalograph (EEG) reference greatly influences the delineation and analysis of EEG scalp recordings, and has attracted much attention in brain electrophysiology research (Hagemann et al., 2001; Nunez et al., 1999). In EEG scalp recording, only the potential difference between two points can be measured, meaning that the use of an appropriate reference is vital (Geselowitz, 1998). Several different types of reference, including the vertex reference (CZ), the linked mastoids reference (LM), the average reference (AR) and the left mastoid reference (L), are currently used for EEG measurement. However, all of these references

may introduce an undesired temporal bias since no neutral point exists on the body surface. Thus, the reference signal itself may involve physiological dynamic processes that will inevitably influence the data. Previous studies have examined the effects of reference choice on EEG data using several methods, including the estimation of the effect of head surface on recordings using AR (Jugnhöfer et al., 1999), the examination of coherence and reference signals (Nunez et al., 1997; Essl and Rappelsberger, 1998; Nunez and Srinivasan 2006) and the investigation of brain asymmetry (Hagemann et al., 2001).

To entirely resolve the problems involved in using body surface points for referencing, a reference with neutral potential is required. Theoretically, a point at infinity is far from brain sources, and has an ideally neutral potential. Therefore, a point at infinity constitutes an ideal reference (infinity reference, IR). In 2001, Yao (2001) proposed a 'reference electrode standardisation technique

* Corresponding author.

E-mail address: dyao@uestc.edu.cn (D. Yao).

(REST) to approximately transform EEG data recorded with a scalp point reference to recordings using an infinity reference (IR; the software for REST transformation can be downloaded at www.neuro.uestc.edu.cn/rest; a simplified MATLAB version can be found in [Supplementary materials](#)). In recent years, the REST has been quantitatively validated through simulation studies with assumed neural sources in both a concentric three-sphere head model (Yao, 2001) and a realistic head model (Zhai and Yao, 2004). These studies have shown that data referenced with REST are more consistent with physiology than data referenced using traditional scalp references. This has been shown using a variety of techniques, including EEG spectral imaging (Yao et al., 2005), EEG coherence (Marzetti et al., 2007), brain evoked potentials (EP) and spatiotemporal analysis (Yao et al., 2007).

However, previously reported studies on EEG electrode reference effects have predominantly focussed on power spectra or spatiotemporal analysis in certain frequency bands. Relatively few studies have investigated the effects of reference choice on other EEG bands. Recently, an increasing number of studies have examined functional connectivity networks in the brain. In particular, a great deal of research attention has focussed on connectivity during the resting state (Buckner and Vincent, 2007; Pawela et al., 2008; Honey et al., 2009), because brain activity in the resting state (in the absence of task stimuli) plays a fundamental role in both simple and complex cognitive processes. Many researchers regard the resting state as the ‘default mode’, in terms of neural network functioning (Raichle et al., 2001; Raichle and Snyder, 2007). In recent years, the default mode network (DMN) has been primarily investigated using functional magnetic resonance imaging (fMRI) (Greicius et al., 2003; Friston, 1994; Buckner and Vincent, 2007), while few studies of the DMN have used EEG measures. Chen et al. (2008) reported an EEG DMN study, examining the spatial characteristics of power spectra in different resting-state EEG frequency bands. Previous studies in both human and animal brains have revealed that the DMN is a kind of ‘small world network’ with high cluster coefficient and short path length (Sporns et al., 2004; Stam et al., 2007; Bassett and Bullmore, 2006). The choice of electrode reference is a particularly vital issue when EEG-related techniques are used to investigate neural connectivity. As such, the systematic investigation of the effects of reference choice on connectivity measurements is an important research goal.

In this study, we conducted a simulation experiment to test the utility of REST in recovering a true EEG-related connectivity network and to evaluate the relative error (RE) introduced by AR, LM and L references. The four references were then applied to real resting-state EEG to investigate the differences among them, and the deviations caused by AR, LM and L compared with REST in measuring power spectra, coherence and DMN configuration for conventional frequency bands were assessed.

2. Methods

2.1. Re-referencing techniques

2.1.1. Reference electrode standardisation technique

REST is a novel method that builds a bridge between the body reference and the theoretical neutral reference at an infinity point (Yao, 2001; Yao et al., 2005). For an IR, the forward EEG calculation is given by

$$V = GS \quad (1)$$

where G is the transfer matrix referenced at infinity, only dependent on the head model, source configuration and electrode montage; S is the distributed source; and V is the scalp EEG recording with a reference at infinity generated by S . Scalp noise is not considered in this model and is assumed to be zero.

For the CZ referenced recordings V_{CZ} , we similarly have

$$V_{CZ} = G_{CZ}S \quad (2)$$

where G_{CZ} is the EEG lead-field matrix with CZ reference and V_{CZ} refers to EEG scalp recordings referenced at CZ. A minimum norm solution (MNS) for the source distribution S is given by

$$S = G_{CZ}^{-}V_{CZ} \quad (3)$$

where $(G_{CZ})^{-}$ denotes the Moore–Penrose generalised inverse of matrix G_{CZ} .

From Eqs. (2) and (3), we can see that the source S is the same, which reflects the fact that reference choice does not influence the source localisation, that is, activated neural sources in the brain are not affected by the particular reference used (Pascual-Marqui and Lehmann, 1993). The potential with reference at infinity can thus be reconstructed as the following:

$$V_{REST} = G(G_{CZ}^{-}V_{CZ}) = UV_{CZ} \quad (4)$$

where $U = GG_{CZ}^{-}$ is the final transfer matrix simultaneously determined by the lead-field matrix G and G_{CZ} , where G is known and G_{CZ} can be easily derived from G . In addition, recordings using any other single electrode as reference can be mathematically transformed to the IR using a formula similar to Eq. (4). This approach differs only in the use of a specific lead-field matrix corresponding to the adopted reference.

Because the potential produced by any source can be equivalently produced by a source distribution enclosing the actual sources (Helmholtz, 1853; Yao, 2003; Yao and He, 2003), we may assume an equivalent source distribution (ESD) on the cortical surface that encloses all possible neural electric sources inside and assume that S in Eqs. (1) and (2) is ESD, instead of the actual neural electric sources. Moreover, ESD may be a closed radial dipole layer. As such, the REST method is actually a model-based extrapolation determined by four factors: the volume conductor model, the equivalent source model, the electrode montage and the calculation of the general inverse.

For the REST method in this study, the head model for all cases was a three-concentric-sphere model. The normalised radii of the three concentric spheres were 0.87 (inner radius of the skull), 0.92 (outer radius of the skull) and 1.0 (radius of the scalp). The normalised conductivities were 1.0, 0.0125 and 1.0 for the brain, skull and scalp, respectively. The centre of the spheres was defined as the coordinate origin. The x -axis was oriented from the origin to the direction of the right ear, and the y -axis was oriented in the posterior–anterior direction. The z -axis was oriented from the origin to the vertex. The equivalent source distribution model was assumed to be a discrete equivalent dipole layer on a closed surface formed by a spherical cap surface with radius of 0.869, above a transverse plane at $z = -0.076$. A discrete approximation of the closed surface was also assumed, consisting of 2600 nodes on the spherical cap surface and 400 nodes on the transverse plane (Yao, 2001). A total of 3000 radial dipoles perpendicular to the enclosed equivalent layer were used to calculate the lead-field matrix. The electrode montage was the same as the EGI (Electrical Geodesics, Inc.) collecting system with 129 electrodes.

In the simulation, a low-density EEG montage consisting of 20 electrodes was selected from the EGI 129 system approximating the standard 10–20 system locations to test the effects of electrode number on REST. Moreover, different conductivity ratios (CRs) between brain and skull were also used to estimate the effects of the volume conductor on REST.

2.1.2. AR reference, LM reference and L reference

The EGI system typically uses the CZ (vertex) electrode as the reference. For the simulated data with an original IR, it is easy to translate data to recordings using CZ as the reference by subtract-

ing the CZ channel signal from each other channel (Yao et al., 2005). The vertex is an electrically active site that can introduce unexpected activity to the referenced recordings. The use of the CZ reference has been deemed inappropriate by some researchers, discouraging its use in EEG analysis (Hagemann et al., 2001; Yao et al., 2007). Therefore, the CZ reference is not considered in our study. Instead, the AR reference, the LM reference, the L reference and REST were transformed from the CZ reference. Details of the transformation from the CZ reference to the AR, LM and L references can be found in the study by Yao et al. (2005).

2.2. Coherence and network construction

2.2.1. Coherence

Coherence is the most common measure used in the analysis of co-operative, synchrony-defined cortical neuronal assemblies (Nunez et al., 1997; Sarnthein et al., 1998; Pereda et al., 2005). Coherence represents the linear relationship at a specific frequency between two signals $x(t)$ and $y(t)$, which can be expressed as:

$$C(f) = \frac{|C_{XY}(f)|^2}{C_{XX}(f)C_{YY}(f)} \quad (5)$$

where $C_{XY}(f)$ is the cross-spectrum between $x(t)$ and $y(t)$, and $C_{XX}(f)$, $C_{YY}(f)$ are the auto spectra calculated from a fast Fourier transform (FFT) performed on $x(t)$ and $y(t)$.

2.2.2. EEG network construction and topography

Different from coherence that can reflect changes in synchronisation and the interaction between two brain regions, brain networks can be used to describe the connectivity among multiple regions or nodes. In this study, an EEG scalp network was constructed using the coherence between nodes as the weight of connectivity, producing a weighted network. For the analysis of both the simulated and real data, 18 nodes were selected from the 129 channels in the EGI montage. These nodes were labelled Ch24, Ch14, Ch11, Ch25, Ch124, Ch34, Ch122, Ch37, Ch105, Ch46, Ch109, Ch62, Ch53, Ch87, Ch59, Ch92, Ch72 and Ch77, approximating the 20 standard electrode locations (Fp1, Fp2, Fz, F3, F4, F7, F8, C3, C4, T7, T8, Pz, P3, P4, P7, P8, O1 and O2) in the 10–20 system.

For the weighted network we generated, a connectivity threshold was set to remove weak links between nodes. To give a better representation of network connectivity topography, we gradually increased the connectivity threshold to decrease the network degree, which refers to the mean links of the whole nodes in the network, until the degree of each network corresponding to different references in different frequency bands reached four.

2.3. Simulation

The effectiveness of REST to reconstruct EEG connectivity was investigated by conducting a simulation study.

2.3.1. Simulation protocol

In the simulation, 100 dipole-pair configurations, each consisting of two unit radial dipoles randomly positioned within the upper hemisphere (radius 0.87), were analysed.

The temporal process of dipolar neural source was simulated using a damped Gaussian function,

$$h(t_i) = \exp\left(-\left(2\pi f \frac{t_i - t_0}{\gamma}\right)^2\right) \cos(2\pi f(t_i - t_0) + \alpha) \quad (6)$$

$i = 1, \dots, k$

with parameters $t_0 = 35 * dt$, $f = 10$ Hz, $\gamma = 5$, $\alpha = \pi/2$ for one dipole in the pair, and $t_0 = 40 * dt$, $f = 10$ Hz, $\gamma = 4$, $\alpha = \pi$ for the other. In this way, two coherent dipoles were generated.

Using Eq. (6) and the above forward model Eqs. (1) and (4), we derived 129-channel spatiotemporal recordings V , V_{AR} , V_{LM} , V_L and V_{REST} . Based on these referenced recordings, the coherence calculating formula (5) was used to calculate the coherence coefficients at 10 Hz among channels. C , C_{AR} , C_{LM} , C_L and C_{REST} were the coherence coefficients corresponding to different references.

2.3.2. RE for coherence

The RE was used to evaluate the effectiveness of each reference, calculated as:

$$RE = \|C - C_*\|/\|C\| \quad (7)$$

where C was the coherence coefficient matrix (129^*129) between channel pairs in 10 Hz referenced at infinity, and C^* was an alternative of the coherence coefficient matrix C_{AR} , C_{LM} , C_L as well as the C_{REST} calculated with REST. The matrix norm $\|*\|$ meant the Frobenius norm defined as:

$$\|C\| = \left(\sum_{i=1}^N \sum_{j=1}^N c_{ij}^2\right)^{1/2} \quad (8)$$

where N represents the total electrode number, and c_{ij} denotes the coherence between channel i and channel j .

2.3.3. Effect of electrode number

We examined the effect of electrode number on REST by comparing the performance of a 20-electrode with a 129-electrode configuration. Eighteen of the 20 electrodes were the same as those mentioned above, which were approximations to standard 10–20-system locations. The other two channels were located at the left and right mastoids.

2.3.4. Effects of volume conductor model

We took 80 as the brain-to-skull CR in the forward calculation to generate the original EEG using an IR. The effects of the volume conductor model on the performance of REST were evaluated by varying CR from 10 to 500 during the REST calculation.

2.4. Application to resting-state EEG

2.4.1. EEG recording and re-referencing

Fifteen healthy right-handed male students (18–30 years old) from the University of Electronic Science and Technology of China volunteered to take part in our study. The experiments were performed in a quiet, air-conditioned laboratory with soft natural light, and maintained at 20–25 °C. Participants were seated and asked to keep their eyes closed for 3 min. A 129-channel EEG was recorded with an EGI system using Ag/AgCl electrodes (including two electrooculography (EOG) channels) with the vertex reference. EEG recordings were sampled online at 500 Hz and filtered with a band-pass filter of 0.1–45 Hz. All impedances were kept below 40 k Ω during the experiments.

Linear-detrending was performed, and EEG data were visually inspected for common artefacts such as eye blinks, eye movements and muscle activity. Furthermore, automated rejection was performed using the amplitude criteria of an absolute voltage threshold (65 μ V), and 10-s epochs without artefacts were chosen for analysis. Eighteen data channels on the outermost ring of electrodes on the inferior surface of the head were eliminated from the study due to recording artefacts caused by an insufficient scalp/sensor contact, leaving 111 electrodes (Srinivasan et al., 1998). EEG data originally recorded using a CZ reference were re-referenced offline to the following references: the IR (REST), the AR reference, the LM reference and the L reference. Transformations between CZ, AR, LM and L references can be easily performed using conventional methods (Yao et al., 2005).

2.4.2. DMN

Previous studies have typically only reported the effect of reference choice on particular bands, such as the alpha band (Hagemann et al., 2001; Yao et al., 2005). Due to the uneven power distribution across different bands, reference choice may have distinct effects on different bands. In the current study, we systemically examined the effects of reference choice on traditional EEG bands, using measures of power spectra, coherence and network connectivity. The bands were defined in a conventional EEG sense: delta (0.5–3.5 Hz), theta (4–7 Hz), alpha-1 (7.5–9.5 Hz), alpha-2 (10–12 Hz), beta-1 (13–23 Hz), beta-2 (24–34 Hz) and gamma (35–45 Hz). The following analysis is based on these seven EEG frequency bands.

2.4.2.1. Power spectra and spatial distribution. EEG artefact-free data were subjected to FFT analysis to obtain the power of each frequency band. Power values and scalp distribution were used to demonstrate the basic information of resting-state EEG, obtained from four different reference types.

2.4.2.2. Spectra amplitude weight centre (AWC). Amplitude weight centre (AWC) reflects the systematic properties of global power. A previous study reported a significant effect of reference choice on the AWC of the alpha band (Yao et al., 2005). In the current study, we additionally used AWC as a measure to test the effects of reference choice on the systematic features of other frequency bands. We defined AWC as

$$X_c(j) = \frac{\sum_{i=1}^N x_i A_i(j)}{\sum_{i=1}^N A_i(j)}, \quad Y_c(j) = \frac{\sum_{i=1}^N y_i A_i(j)}{\sum_{i=1}^N A_i(j)}, \quad Z_c(j) = \frac{\sum_{i=1}^N z_i A_i(j)}{\sum_{i=1}^N A_i(j)} \quad (9)$$

where $A_i(j)$ is the square root of the power of the frequency band j at electrode i . ($X_c(j)$, $Y_c(j)$, $Z_c(j)$) are the coordinates of the AWC; N is the number of electrodes, and (x_i, y_i, z_i) are the coordinates of the electrodes.

2.4.2.3. DMN construction and graphic analysis. The same 18 nodes were selected and the coherence between nodes was calculated as the weight of DMN connectivity. The weighted density of the network, used to evaluate the intensity and efficiency of the network links (De Vico Fallani et al., 2008), was defined as:

$$E = \frac{1}{N(N-1)} \sum_{i \neq j} w_{ij} \quad N = 18; i, j = 1, \dots, 18 \quad (10)$$

where N is the node number and w_{ij} is the weight between node i and j . Network density represents connectivity strength, global information integration and processing capacity, which greatly depends on coherence here.

3. Results

3.1. Simulation results

It is obvious from Fig. 1(a) that the different references resulted in different REs. REST generated the smallest error, with the mean RE of the whole dipole-pair 0.062%, while the mean RE reached 16.61% with L, and 9.73% and 15.47% with AR and LM, respectively. A Tukey's test revealed significant differences for all pair-wise comparisons among these references ($P = 0.002$ for LM vs. L; $P < 0.001$ for other pairs).

The relative error after reducing the electrode number is shown in Fig. 1(b). It can be seen that the REST still introduced the smallest error (mean RE: 3.05%), while the mean error produced by AR was 11.57%. The errors produced by LM (mean RE: 15.60%) and L (mean RE: 17.35%) were larger than those obtained using REST and AR. However, the errors of both LM and L were slightly altered, while AR and REST produced larger error compared with that of the 129 electrodes. Overall, REST showed the best performance with the smallest errors. A Tukey's test revealed significant differences for all pair-wise comparisons among these references ($P = 0.001$ for LM vs. L; $P < 0.001$ for other pairs).

The RE of REST with various CRs can be seen in Fig. 2. Fig. 2(a) shows the results with the four different CRs (20, 40, 60 and 80). It indicated that the largest error occurred at CR = 20 with an average RE = 0.13% over the 100 dipole-pair sources. Fig. 2(b) shows the averaged RE of coherence for CRs from 20 to 500. Moreover, it shows that REST was robust to CR value in a wide range. Comparing to Fig. 1, Fig. 2 reveals that the errors introduced by the head models were much smaller than those caused by the non-zero references AR, LM or L.

One dipole-pair of the 100 randomly positioned dipole-pairs was selected to display scalp connectivity over 18 nodes in the case of 129 channels involved in reference transformation. The connectivity networks produced by different reference types are shown in Fig. 3.

The spatial coordinates for these two dipoles were (−0.62, −0.21, 0.425) and (0.62, 0.37, 0.425). One dipole was located at the left occipital area, while the other was located at the right frontal area. The network generated by measuring EEG coherence with the original IR revealed high-density connectivity between left occipital and right frontal areas, showing high connectivity around the source position. Moreover, connectivity between the two areas also reflected the coherence existed between the two sources.

The REST network showed similar configuration to an IR network, while the results obtained using other reference types (AR, LM and L) showed substantial bias.

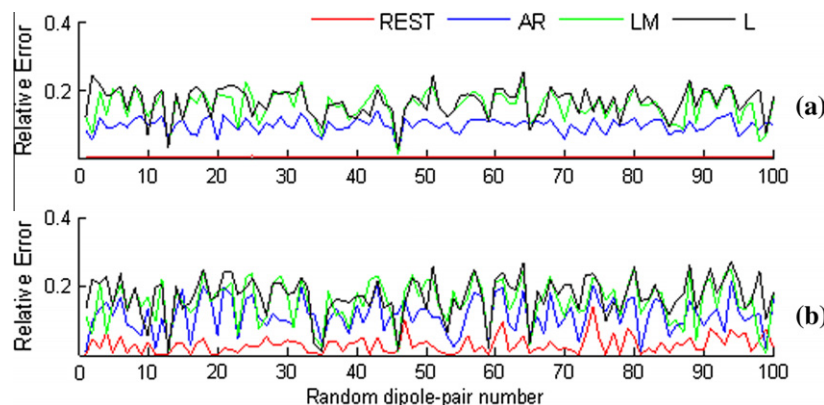


Fig. 1. The relative error (RE) of the coherence with four references for all the dipole-pairs using 129 (a) or 20 (b) scalp locations.

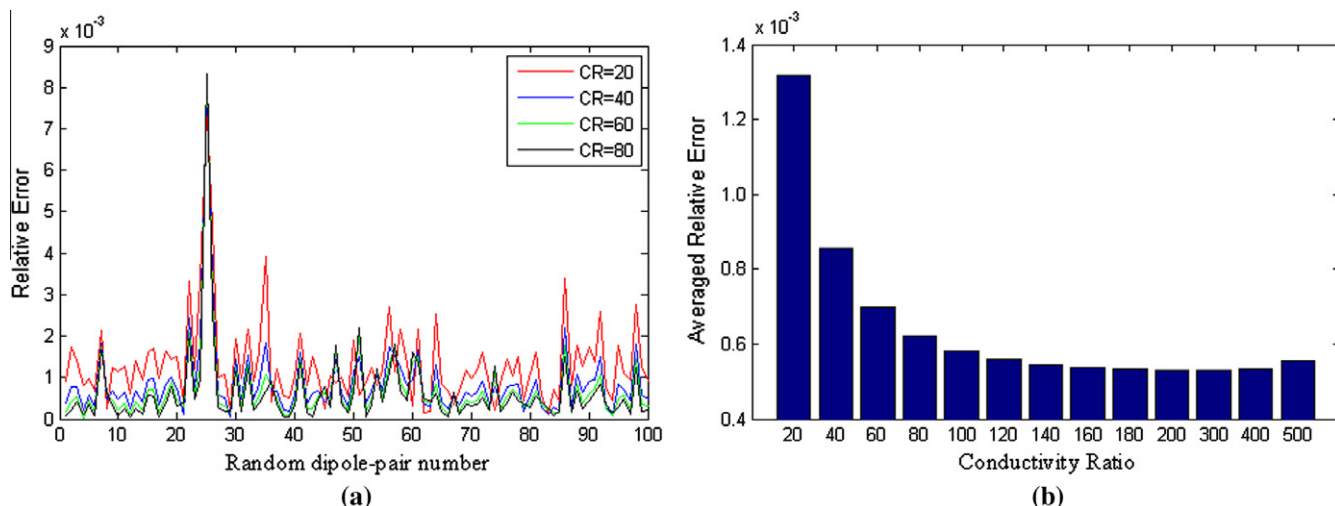


Fig. 2. (a) The relative error (RE) of the coherence with REST, using conductivity ratio = 80 to generate the original scalp EEG, and CR ranging from 20 to 80 in REST. (b) The averaged relative error of the coherence over the 100 dipole-pair sources for different CRs (20 ~ 500) when the true CR = 80.

3.2. Resting-state EEG analysis

3.2.1. Power spectra

Fig. 4 shows the absolute power values of different frequency bands. It can be seen that the choice of reference had distinct effects on different power bands. Across the different references, L consistently showed the largest values, while AR consistently showed the smallest. In addition, the power distributed in the low- and middle-frequency bands was much higher than that distributed in the high-frequency bands.

One-way repeated-measures analyses of variance (ANOVAs) were performed on the absolute power values for each frequency band to evaluate the reference effects. Significant differences revealed by ANOVA were further analysed for multiple comparisons using Tukey's *post hoc* test. The value of epsilon (ϵ) of Greenhouse–Geisser would be denoted when the Greenhouse–Geisser correction was necessary. A significance level of $P < 0.05$ was used in all comparisons. These statistics revealed significant differences for all frequency bands (delta: $F(3, 42) = 29.262$, $\epsilon = 0.479$; $P < 0.001$; theta: $F(3, 42) = 91.653$, $P < 0.001$; alpha-1: $F(3, 42) = 35.713$, $\epsilon = 0.544$;

$P < 0.001$; alpha-2: $F(3, 42) = 46.558$, $\epsilon = 0.429$; $P < 0.001$; beta-1: $F(3, 42) = 52.913$, $\epsilon = 0.556$; $P < 0.001$; beta-2: $F(3, 42) = 11.383$, $\epsilon = 0.443$; $P = 0.002$; gamma: $F(3, 42) = 11.276$, $\epsilon = 0.394$; $P = 0.003$). In addition, pair-wise multiple comparisons revealed significant differences (Tukey's test, $P < 0.05$) for all comparisons, except between LM and L for alpha-1 and alpha-2.

Fig. 5 illustrates the spectral topography mapping in different frequency bands for REST (a), AR (b), LM (c), L (d), AR-REST (e), LM-REST (f) and L-REST (g), respectively. As shown in Fig. 5(a), delta power was primarily distributed over the prefrontal area. The frontal–central and occipital areas were associated with theta-related activity, which showed a clear expansion from anterior to posterior areas. Both alpha-1 and alpha-2 activities were mainly distributed over the posterior area. Beta-1 showed a similar distribution to alpha-1 and alpha-2, but the power over the posterior area was relatively weak. High-frequency beta-2 and gamma-related activities showed a similar distribution that included the frontal and occipital areas, as well as other small discrete areas.

Fig. 5(b)–(d) shows the spectral topographies for AR, LM and L. Although the power distributions for AR and REST were similar, the

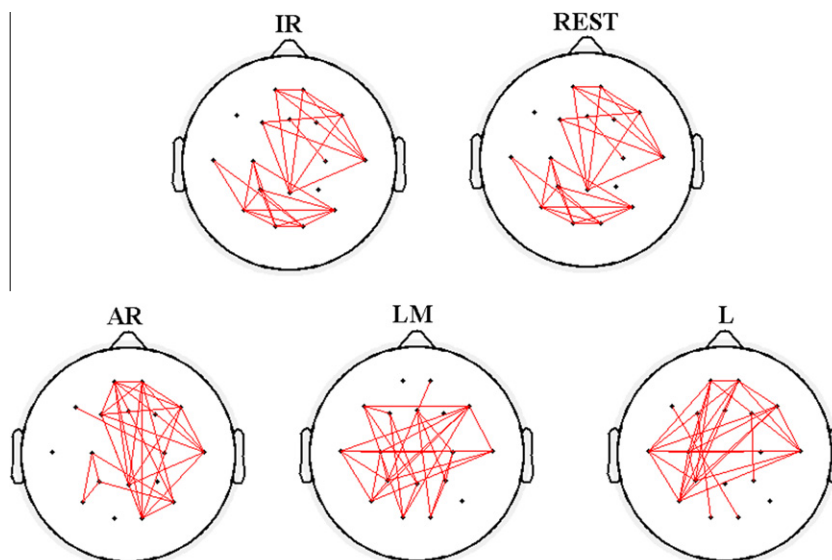


Fig. 3. The network configuration for one dipole-pair with different references.

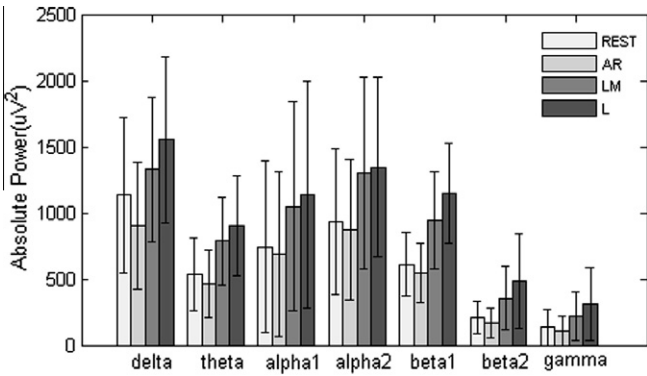


Fig. 4. The absolute power values in all frequency bands with different references. Shown is the average of band powers of all channels over 15 subjects.

power values for each region were nevertheless distinct, which is clearly demonstrated from the difference topography (e). The spectral topographies for LM and L (c–d) exaggerated the central area

and the right-anterior area for all bands, respectively. The main power distribution areas were largely consistent for all four references. However, substantial differences in the activity strength and extension were found in the same frequency band. This difference is clearly illustrated in Fig. 5(e)–(g) described below.

The difference topographies for each band between AR and REST are shown in Fig. 5(e). Compared with REST, AR had less power over posterior areas, reflecting an anterior shift of the power distribution. Fig. 5(f) shows that the LM reference introduced a large increase of power over anterior areas, and it indicated an obvious frontal shift of power spectra for all frequency bands. However, the topographic difference between L and REST in Fig. 5(g) revealed a large increase of power over the right-anterior region, indicating a strong hemisphere bias.

AWCs were calculated with different references in each frequency band. The AWCs of AR, LM and L references were then compared with that of REST. Fig. 6 shows AWC shifts for AR, LM and L relative to REST, calculated by subtracting the REST AWC from that of the other references. The results were averaged over 15 subjects. We found that LM and L introduced larger shifts than AR. The AWC

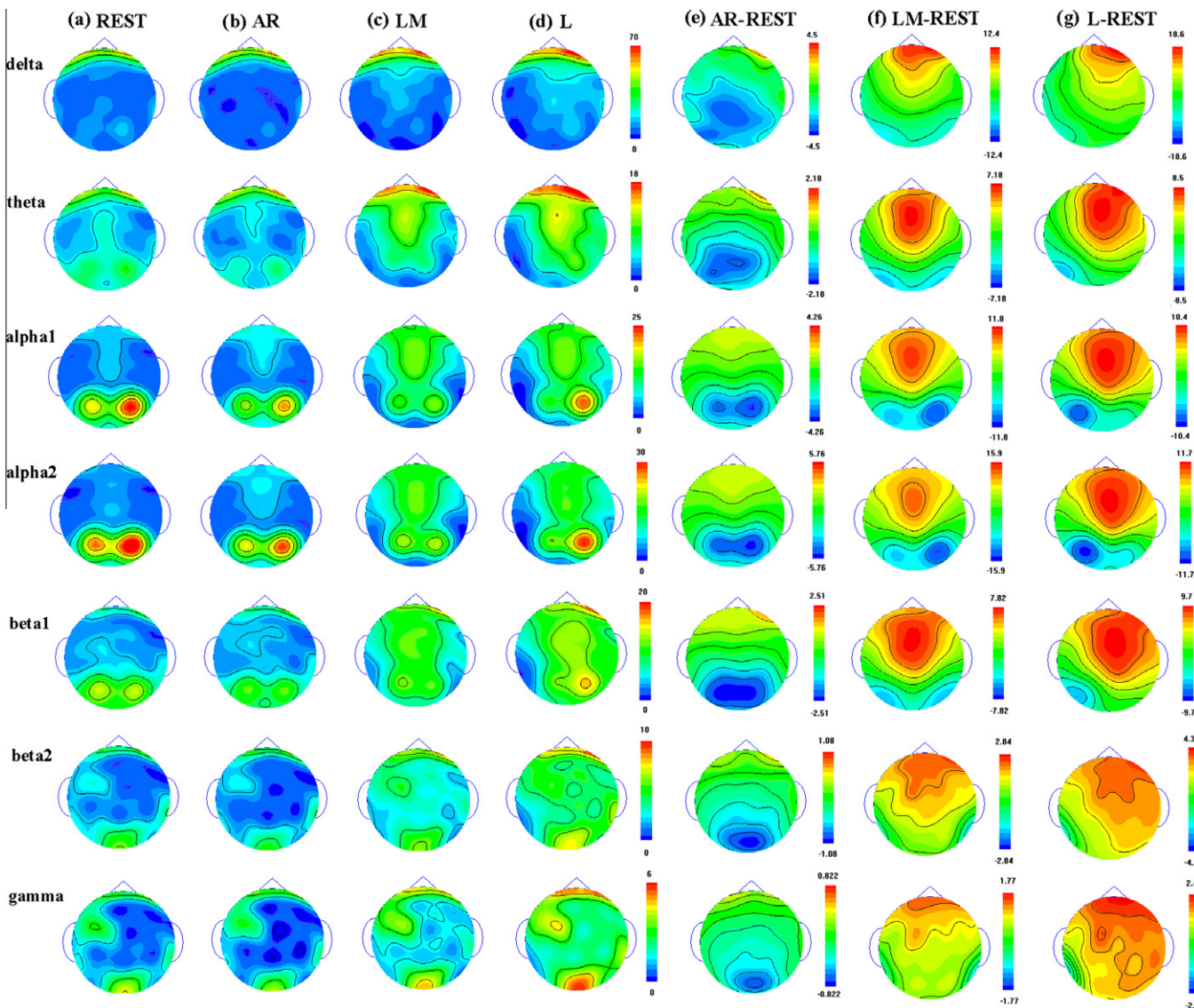


Fig. 5. The spectral distribution mappings in all frequency bands using an infinity reference as estimated by the reference electrode standardisation technique (REST; a); an average reference (AR; b); a linked-mastoid reference (LM; c); a left mastoid reference (L; d), and the spectral distribution differences between AR and IR (e), LM and IR (f), and L and IR (g). The same color bar was adopted for each frequency band (a–d).

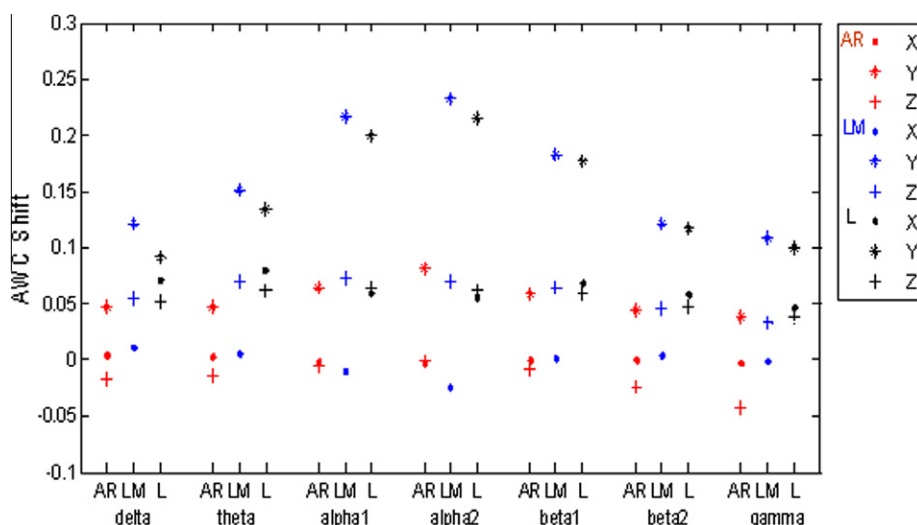


Fig. 6. The AWCs shifts of AR, LM and L in the whole frequency bands. Three coordinate components are displayed with different symbols (□ for x-axis, ○ for y-axis, △ for z-axis) and red, blue and black colors are used for AR, LM and L, respectively. (For interpretation of the references to color in this figure legend, the reader is referred to the web version of this article.)

shifts along x-axis of AR, LM and L were all less than 0.1. Significant AWC differences along the x-axis were found for all four references (delta: $F(3, 42) = 37.835$, $\epsilon = 0.533$; $P < 0.001$; theta: $F(3, 42) = 91.367$, $P < 0.001$; alpha-1: $F(3, 42) = 144.612$, $\epsilon = 0.486$; $P < 0.001$; alpha-2: $F(3, 42) = 55.716$, $\epsilon = 0.628$; $P < 0.001$; beta-1: $F(3, 42) = 112.438$, $\epsilon = 0.469$; $P < 0.001$; beta-2: $F(3, 42) = 294.140$, $\epsilon = 0.520$; $P < 0.001$; gamma: $F(3, 42) = 87.129$, $\epsilon = 0.587$; $P < 0.001$). Pair-wise multiple comparison tests revealed significant differences between LM and the other three references (Tukey's test, $P < 0.05$) along the x-axis. Along the y-axis, the AWC of AR, LM as well as L showed significant anterior shifts in all frequency bands compared with REST, especially for the middle-frequency bands including alpha-1, alpha-2 and beta-1. One-way repeated-measures ANOVAs were performed, revealing that the AWC difference among the four references along the y-axis was significant (delta: $F(3, 42) = 184.467$, $\epsilon = 0.501$; $P < 0.001$; theta: $F(3, 42) = 365.215$, $\epsilon = 0.678$; $P < 0.001$; alpha-1: $F(3, 42) = 74.753$, $\epsilon = 0.708$; $P < 0.001$; alpha-2: $F(3, 42) = 178.283$, $\epsilon = 0.503$; $P < 0.001$; beta-1: $F(3, 42) = 286.853$, $\epsilon = 0.659$; $P < 0.001$; beta-2: $F(3, 42) = 52.849$, $\epsilon = 0.651$; $P < 0.001$; gamma: $F(3, 42) = 140.674$, $\epsilon = 0.380$; $P < 0.001$). Positive z-axis shifts were found for LM and L, while AR introduced negative shifts along the z-axis. Differences in AWC along the z-axis among the four references were significant in all bands (delta: $F(3, 42) = 190.263$, $\epsilon = 0.382$; $P < 0.001$; theta: $F(3, 42) = 28.105$, $\epsilon = 0.566$; $P < 0.001$; alpha-1: $F(3, 42) = 48.236$, $\epsilon = 0.458$; $P < 0.001$; alpha-2: $F(3, 42) = 153.227$, $\epsilon = 0.602$; $P < 0.001$; beta-1: $F(3, 42) = 18.913$, $\epsilon = 0.567$; $P < 0.001$; beta-2: $F(3, 42) = 29.189$, $\epsilon = 0.538$; $P < 0.001$; gamma: $F(3, 42) = 67.200$, $\epsilon = 0.503$; $P < 0.001$).

3.2.2. DMN weighted density

The weighted density of the DMN averaged across 15 subjects for all frequency bands is shown in Fig. 7.

Among the four references, L and LM showed the largest weighted density, with high variability. For REST and AR, the weighted density of the middle-frequency bands was much higher than that of the low- and high-frequency bands. For L and LM, however, the weighted density increased dramatically, particularly in the high-frequency bands. One-way repeated-measures ANOVA revealed that differences among the four references were significant in all frequency bands (delta: $F(3, 42) = 11.982$, $\epsilon = 0.683$; $P < 0.001$; theta: $F(3, 42) = 53.744$, $\epsilon = 0.527$; $P < 0.001$; alpha-1: $F(3, 42) = 51.630$, $\epsilon = 0.500$; $P < 0.001$; alpha-2: $F(3, 42) = 22.370$,

$\epsilon = 0.504$; $P < 0.001$; beta-1: $F(3, 42) = 32.788$, $\epsilon = 0.410$; $P < 0.001$; beta-2: $F(3, 42) = 26.025$, $\epsilon = 0.421$; $P = 0.001$; gamma: $F(3, 42) = 25.196$, $\epsilon = 0.416$; $P = 0.001$). A pair-wise comparison, however, revealed that the difference between AR and REST in theta and beta-2 bands was not significant (Tukey's test, $P > 0.05$).

3.2.3. DMN connectivity topography

Fig. 8 shows the networks of four degrees with the four references in different frequency bands, with the color lines representing the level of the connectivity weights.

It is obvious from Fig. 8 that the network configurations varied profoundly across different references. The first column shows that high-density connectivity prevailed over the posterior regions in low- and high-frequency bands for REST, and long-distance connectivity bridged between anterior and posterior areas in the middle-frequency bands, whereas the connectivity topographies of AR and REST were highly comparable in the alpha-2 band. Long-distance connectivity from anterior to posterior areas was enhanced in all frequency bands with AR. Revealing a substantial number of null-degree nodes, the connectivity of LM and L was more focal and sparse indicating that a strong bias was introduced by LM and L. With these mastoid references, the connectivity over the posterior area was weakened and the connectivity over the anterior area was enhanced. Particularly for the unilateral mastoid reference, the

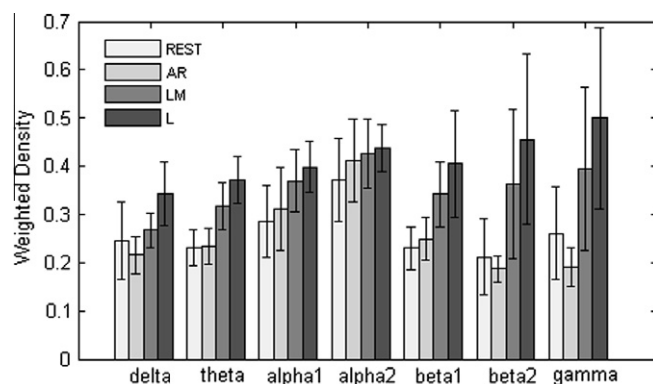


Fig. 7. The network weighted-density averaged across 15 subjects in the different frequency bands when different references are used.

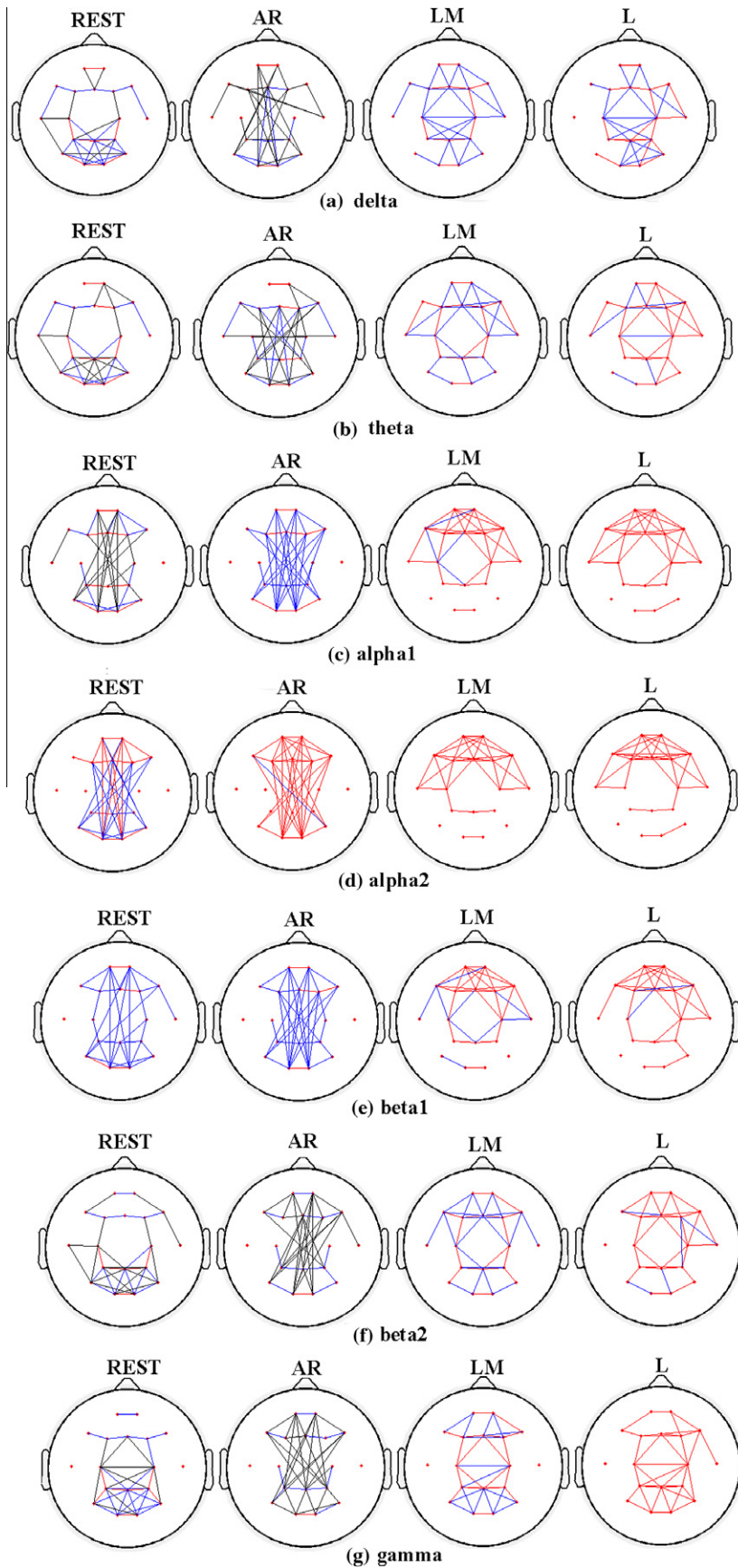


Fig. 8. The EEG default mode network with 18 nodes averaged across 15 subjects. The degree of each network is 4. The 18 red points stand for network nodes. The red line (connectivity weight ≥ 0.6), the blue line ($0.6 \geq \text{connectivity weight} \geq 0.4$), and the black line (connectivity weight ≤ 0.4) denote different connectivity levels. (For interpretation of the references to color in this figure legend, the reader is referred to the web version of this article.)

network connectivity in the immediate vicinity of the reference location was severely reduced. Thus, the reference-dependent effect is clear in the network topography.

4. Discussion

4.1. Simulation analysis

The simulation results showed that the relative error of coherence was greatly reduced by REST. Irrespective of the dipole-pair locations, the RE level of the four references was significantly different. Although the RE introduced by AR was smaller compared with mastoid references (LM and L), the network configuration was still markedly distorted by AR, which was in striking contrast to REST, lacking notable distortions. These results strongly suggest that the effects of using different EEG references have a profound impact on the data analysis. When the electrode number was reduced to 20, the RE of REST was still significantly smaller compared with the other reference schemes (AR, LM and L), underscoring the validity of REST even for a low-density montage, although the spatially under-sampled EEG montage yielded a larger RE compared with the findings for 129 electrodes. The reference effects of LM and L were barely affected by number of electrodes. However, the RE introduced by AR was substantially increased compared with that of 129 electrodes and demonstrated the fact that the AR is only effective with a sufficient number of electrodes. Given these simulation findings, REST was considered as a standard for evaluating the reference effects for the resting-state EEG.

Besides the electrode montage, REST also depended on the head model. However, this dependency was relatively weak. For the practically meaningful situations: CR = 15 (Oostendorp et al., 2000) ~ 80 (Rush and Driscoll, 1969), even the assumed CR is different from the true value; the REs always remained at a level of 10^{-3} . In addition, the RE of REST was smaller than that of AR, LM and L regardless of the particular conductivity ratio used (Fig. 2).

4.2. Application to real data

4.2.1. Spectra analysis

We investigated the possible effects of four references on the power spectra, in terms of power values and power distribution. The results revealed that reference choice influenced two aspects of power spectra: magnitude and distribution.

Due to the special frequency dynamic activity, the influence of reference on power spectra varied across frequency bands. Fig. 4 shows that there was a significant effect of reference on power values. Across all frequency bands, the LM reference produced the largest absolute power values, whereas the AR rendered the smallest power values. This finding confirms that these differences should be taken into account during the study of physiological processes (Yao et al., 2005). There were also distinct topographic differences of absolute power among the references as shown in Fig. 5. More concentrated alpha activities were revealed in the posterior area with REST compared with AR, LM and L. Activities remarkably decreased in the posterior area with AR, whereas activities dramatically increased in the anterior area with LM and L, and these variations all showed clear anterior shifts. With L, activations over the right-anterior area were strengthened. The AWC shifts in Fig. 6 were consistent with the topographic differences in Fig. 5, and the frontal shifts induced by LM and L were much larger than those induced by AR. Moreover, the right hemisphere shift with L was obvious, evidently resulting from the lateralised position of the reference electrode.

4.2.2. Coherence and DMN analysis

Coherence is another spectra-related variable, and was substantially affected by reference choice. L and LM showed much larger coherence amplitude than AR and REST. The results clearly demonstrated that the choice of an active scalp reference site led to large coherence distortions. Previous studies have reported that scalp EEG coherence can be simultaneously influenced by volume conduction and reference choice (Nunez et al., 1997; Nunez and Srinivasan, 2006), and the increasing reference activity leads to a falsely increased coherence (Essl and Rappelsberger, 1998). The large potential of LM and L reference signals strongly influences original EEG data by introducing new components. Accordingly, the LM and L references in our study generated large changes in coherence values and network weighted density.

The DMN connectivity topography mappings shown in Fig. 8 illustrate the influence of reference choice on scalp network connectivity. In terms of topography, both AR and REST showed tight connectivity between posterior and anterior areas; however, networks using L and LM references were found to be relatively invalid because no strong connectivity was shown between these two areas. Moreover, network connectivity over posterior areas was considerably weaker when LM and L references were used, and connectivity around the left mastoid was reduced with L, revealing the shortcomings of using single or two-site references. It is also clearly shown in our results that AR augmented the long-distance connectivity between anterior and posterior areas in all frequency bands. The connectivity configuration distortion may be influenced by the frontal and downward spectra shift with AR.

Our results demonstrated that the middle-frequency bands (alpha-1, alpha-2 and beta-1) have strong connectivity between the anterior and posterior areas in DMNs with REST and AR references. This connectivity represented the strong information exchange between frontal and occipital areas. This was not revealed using L and LM references.

4.3. Comparisons of the four references

The above comparisons consistently confirmed the obvious effects of references on power spectra, coherence and DMN, confirming the necessity of choosing a suitable reference in EEG studies. Generally, the differences we found were due to the inherent properties of the different references. We found the L and LM produced stronger power and higher coherence values than the other two references. As the mastoids are closer to the occipital regions, they may have a greater effect on the power of occipital electrodes than the frontal electrodes, resulting in a shift and extension to the anterior regions compared with REST and AR references. When L was used, the channels close to the reference electrode were particularly strongly influenced. The strength of the left-posterior area thus declined, whereas the strength of the right-anterior area was increased. It was revealed that the body-surface-related reference influenced those electrodes nearby to a greater extent, presumably because the reference electrode inherently contains strong activities.

As reported in previous studies (Yao, 2001), because IR is theoretically far from all electrodes, it acts as a reliable neutral reference. The reconstructed IR (REST) is dependent on the assumed volume model, sensor and source configuration. In the current study, REST was implemented using a unified three-shell sphere head model. Although a realistic head model constructed for each individual subject would likely improve the accuracy of REST for each subject, the simulation study in this work and those in previous reports (Yao, 2001; Zhai and Yao, 2004) all showed that REST is effective even when the volume conductor differs from the true head model. It was shown in the simulation that RE is greatly reduced with REST compared with other commonly used references.

Therefore, REST may be regarded as an appropriate standard for evaluating AR, LM and L and other physical references in practice to determine the possible distortion that is caused by particular non-zero references.

Comparing AR, LM and L references revealed that AR produced results that were much closer to those of REST, when applied to both simulated and real resting-state EEG data. These findings indicated that AR is a better choice than LM and L, which have been adopted in recent neurocognitive EEG studies. The REST accuracy will be affected by the head model, electrode number (Yao, 2001), whereas the AR is limited by the assumption that head electrode sampling is able to approximate a closed integral over the head surface (Nunez and Srinivasan, 2006), that is, the AR is commonly recommended as a neutral and valid reference in cases where the scalp field is spatially sampled with a sufficiently large number of sensors (Dien, 1998). However, when compared with REST, AR is still far from the ideal neutral reference. This is due not only to inadequate electrode density, but also to the electrode spatial distribution typically being limited to the upper surface. AR approximates zero only when dense electrodes cover the whole surface of the head (Nunez and Srinivasan 2006; Srinivasan et al., 1998; Ferree, 2006). Thus, the lack of facial and inferior electrodes introduces frontal and downward shift when AR is adopted.

4.4. Various reference-free techniques

Many studies focussing on reference-free methods such as scalp Laplacian (SL), the cortical imaging technique (CIT) and the current source density (CSD) transformed method have been published (Nunez et al., 1994; Srinivasan et al., 1998; Yao, 2000; Tenke and Kayser, 2005). SL is both a spatial high-pass band estimate of scalp data and an estimate of local current passing normal to the skull (Nunez and Srinivasan, 2006; Yao, 2002). The cortical imaging is from the scalp to the cortical surface, and because this is an inward extrapolation technique, any error in scalp data or the head model becomes enlarged (Yao, 2000; Yao et al., 2001). By contrast, the operation involved in REST is from 'scalp' to 'scalp'; the noise in data and error in head model will not be enlarged.

In addition, the constant in the spherical spline interpolation formula (Perrin et al., 1987; Yao, 2000; Ferree, 2006) comes primarily from the constant potential introduced by a non-neutral reference. Therefore, the spherical spline fit may be another approach for recovering the reference potential in theory, in addition to the equivalent dipole layer approach in REST. However, the spherical spline fit aims at a smooth spatial interpolation of the non-sampled positions (Perrin et al., 1987), and the inverse indeterminacy is more serious compared with the equivalent dipole layer approach. Moreover, the requirement of regularisation may substantially reduce efficiency in recovering the true spherical spectra (Yao et al., 2001). For these reasons, the equivalent dipole layer approach was adopted in REST (Yao, 2001).

5. Conclusions

In this study, we investigated the effect of reference choice on simulated data as well as real resting-state EEG data, as measured by spectra, coherence and DMN connectivity. The results of the simulation revealed that RE was the smallest when REST was used, while AR, LM and L references introduced a substantially higher level of error. All spectral properties, including power values, spatial distribution and AWC, were found to be distinctly different when alternative references were adopted. Reference choice was also found to have significantly effect on coherence, a measure that indicates synchronisation and interaction. The default mode network was constructed on the basis of coherence. Moreover, the results revealed that refer-

ence choice also influences the network pattern. This finding indicates that the choice of reference plays an important role in functional network studies in the brain, and must be carefully considered. REST is a promising reference technique for objective comparison in cross-laboratory studies and clinical practice.

Acknowledgements

This work was supported by NSFC #60736029, NSFC #30525030, #60701015 and the 863 Project 2009AA02Z301. We thank the two anonymous reviewers for their constructive comments that improved the manuscript considerably.

Appendix A. Supplementary data

Supplementary data associated with this article can be found, in the online version, at doi:10.1016/j.clinph.2010.03.056. The following is available in this Supplementary Material: • Lead_field calculation • REST software • Userguide of matlab REST References.

References

- Bassett DS, Bullmore ET. Small world brain networks. *Neuroscientist* 2006;12:512–23.
- Buckner RL, Vincent JL. Unrest at rest: the importance of default activity and spontaneous network correlations. *NeuroImage* 2007;37:1091–6.
- Chen AC, Feng W, Zhao H, Yin Y, Wang P. EEG default mode network in the human brain: spectral regional field powers. *NeuroImage* 2008;41:561–74.
- De Vico Fallani F, Astolfi L, Cincotti F, Mattia D, Tocci A, Salinari S, Marciani MG, Witte H, Colosimo A, Babiloni F. Brain network analysis from high-resolution EEG recording by the application of theoretical graph indexes. *IEEE Trans Neural Syst Rehabil Eng* 2008;442–52.
- Dien J. Issues in the application of the average reference: review, critiques, and recommendations. *Behav Res Methods Instrum Comput* 1998;30:34–43.
- Essl M, Rappelsberger P. EEG coherence and reference signals: experimental results and mathematical explanations. *Med Biol Eng Comput* 1998;36:399–406.
- Ferree TC. Spherical splines and average reference in scalp electroencephalography. *Brain Topogr* 2006;19(1–2):43–52.
- Friston KJ. Functional and effective connectivity in neuroimaging: a synthesis. *Hum Brain Mapp* 1994;2:56–78.
- Geselowitz DB. The zero of potential. *IEEE Eng Med Biol* 1998;17:128–32.
- Greicius MD, Krasnow B, Reiss AL, Menon V. Functional connectivity in the resting brain: a network analysis of the default mode hypothesis. *Proc Natl Acad Sci USA* 2003;100:253–8.
- Hagemann D, Naumann E, Thayer JF. The quest for the EEG reference revisited: a glance from brain asymmetry research. *Psychophysiology* 2001;38:847–57.
- Helmholtz H. Ueber einige Gesetze der Verteilung elektrischer Ströme in Körperliche Leitern mit Anwendung auf die thierisch-elektrischen. *Versuche Pogg Ann* 1853;89:211–33. 353–377.
- Honey CJ, Sporns O, Cammoun L, Gigandet X, Thiran JP, Meuli R, Hagmann P. Predicting human resting-state functional connectivity from structural connectivity. *Proc Natl Acad Sci USA* 2009;106:2035–40.
- Jugnhöfer M, Elbert T, Tucker DM, Braun C. The polar average reference effect: a bias in estimating the head surface integral in EEG recording. *Clin Neurophysiol* 1999;110:1149–55.
- Marzetti L, Nolte G, Perrucci MG, Romani GL, Grattas CD. The use of standardized infinity reference in EEG coherency studies. *NeuroImage* 2007;36:48–63.
- Nunez PL, Silibertein RB, Cadush PJ, Wijesinghe RS, Westdrop AF, Srinivasan R. A theoretical and experimental study of high resolution EEG based on surface Laplacian and cortical imaging. *Electroenceph Clin Neurophysiol* 1994;90:40–57.
- Nunez PL, Srinivasan R, Westdorp AF, Wijesinghe RS, Tucker DM, Silberstein RB, Cadusch PJ. EEG coherency I: statistics, reference electrode, volume conduction, Laplacians, cortical imaging, and interpretation at multiple scales. *Electroenceph Clin Neurophysiol* 1997;103:499–515.
- Nunez PL, Silberstein RB, Shi Z, Carpenter MR, Srinivasan R, Tucker DM, Doran SM, Cadusch PJ, Wijesinghe RS. EEG coherency II: experimental comparisons of multiple measures. *Clin Neurophysiol* 1999;110:469–86.
- Nunez PL, Srinivasan R. *Electric fields of the brain: the neurophysics of EEG*. 2nd ed. New York: Oxford University Press; 2006.
- Oostendorp TF, Delbeke J, Stegeman DF. The conductivity of the human skull: results of *in vivo* and *in vitro* measurements. *IEEE Trans Biomed Eng* 2000;47(11):1487–92.
- Pascual-Marqui RD, Lehmann D. Topographical maps, sources localization inference, and the reference electrode: comments on a paper by Desmedt et al. *Electroenceph Clin Neurophysiol* 1993;88:532–3.
- Pawela CP, Biswal BB, Cho YR, Kao DS, Li R, Jones SR, Schulte ML, Matloub HS, Hudetz AG, Hyde JS. Resting-state functional connectivity of the rat brain. *Magn Reson Med* 2008;59:1021–9.

- Pereda E, Quiroga RQ, Bhattacharya J. Nonlinear multivariate analysis of neurophysiological signals 2005. *Prog Neurobiol* 2005;77:1–37.
- Perrin F, Pernier J, Bertrand O, Giard MH, Echallier JF. Mapping of scalp potentials by surface spline interpolation. *Electroenceph Clin Neurophysiol* 1987;66:75–81.
- Raichle ME, MacLeod AM, Snyder AZ, Powers WJ, Gusnard DA, Shulman GL. A default mode of brain function. *Proc Natl Acad Sci USA* 2001;98:676–82.
- Raichle ME, Snyder AZ. A default mode of brain function: a brief history of an evolving idea. *NeuroImage* 2007;237:1083–90.
- Rush S, Driscoll DA. EEG electrode sensitivity—an application of reciprocity. *IEEE Trans Biomed Eng* 1969;16(1):15–22.
- Sarnthein J, Petsche H, Rappelsberger P, Shaw GL, Stein A. Synchronization between prefrontal and posterior association cortex during human working memory. *Proc Natl Acad Sci USA* 1998;95:7092–6.
- Sporns O, Chialvo DR, Kaiser M, Hilgetag CC. Organization, development and function of complex brain networks. *Trends Cogn Sci* 2004;8:418–25.
- Srinivasan R, Nunez PL, Silberstein RB. Spatial filtering and neocortical dynamics: estimates of EEG coherence. *IEEE Trans Biomed Eng* 1998;45:814–26.
- Stam CJ, Jones BF, Nolte G, Breakspear M, Scheltens. Small-world network and functional connectivity in Alzheimer's Disease. *Cerebral Cortex* January 2007;17:92–9.
- Tenke CE, Kayser J. Reference-free quantification of EEG spectra: combining current source density (CSD) and frequency principal components analysis (fPCA). *Clin Neurophysiol* 2005;116:2826–46.
- Yao D. High-resolution EEG mappings: a spherical harmonic spectra theory and Simulation results. *Clin Neurophysiol* 2000;111:81–92.
- Yao D. A method to standardize a reference of scalp EEG recordings to a point at infinity. *Physiol Meas* 2001;22:693–711.
- Yao D, Zhou Y, Zeng M, Fan S, Lian J, Wu D, Ao X, Chen L, He B. A study of equivalent source techniques for high-resolution EEG imaging. *Phys Med Biol* 2001;46(8):2255–66.
- Yao D. The theoretic relation of scalp Laplacian and scalp current density of a spherical head model. *Phys Med Biol* 2002;47:2179–85.
- Yao D. High-resolution EEG mapping: an equivalent charge-layer approach. *Phys Med Biol* 2003;48:1997–2011.
- Yao D, He B. Equivalent physical models and formulation of equivalent source layer in high-resolution EEG imaging. *Phys Med Biol* 2003;48:3475–83.
- Yao D, Wang L, Oostenveld R, Nielsen KD, Arendt-Nielsen L, Chen A. A comparative study of different references for EEG spectral mapping: the issue of the neutral reference and the use of the infinity reference. *Physiol Meas* 2005;6:173–84.
- Yao D, Wang L, Arendt-Nielsen L, Chen AC. The effect of reference choices on the spatio-temporal analysis of brain evoked potentials: the use of infinite reference. *Comput Biol Med* 2007;37(11):1529–38.
- Zhai Y, Yao D. A study on the reference electrode standardization technique for a realistic head model. *Comput Methods Programs Biomed* 2004;76:29–238.